**Proceedings of the ASME International Mechanical Engineering Congress and Exposition**
**IMECE 2014**
**November 14-20, 2014, Montreal, CANADA**

**IMECE2014-38834**

# STATIC MODELING OF A BI-AXIAL MICRO-MIRROR WITH SIDEWALL ELECTRODES

**Shahrzad Towfighian** *
Department of Mechanical Engineering
State University of New York at Binghamton
Binghamton, New York 13902
Email:stowfigh@binghamton.edu

**Mehmet Ozdogan**
Department of Mechanical Engineering
State University of New York at Binghamton
Binghamton, New York 13902
Email: mozdoga1@binghamton.edu

## ABSTRACT

*The static modeling of a bi-axial torsional micro-mirror with sidewall electrodes is investigated. The mirror and sidewall electrodes experience different voltages. As a result of the potential difference, the mirror rotates about x and y axes with the torques generated from electrostatic forces by the sidewall and bottom electrodes. The rotations about two axes are made possible using a gimbal frame and serpentine springs. An analytical model is presented that is a simplified model of a previous study based on independent excitation of the two rotation angles. The simplified model enables prediction of the rotation angles with good accuracy and faster computation time.*

## 1 INTRODUCTION

Micro-electromechanical systems (MEMS) are becoming mainstream using recent microfabrication methods (e.g Silicon bulk micro-machining, surface micro-machining [1]). Biaxial micro-mirrors are among MEMS devices adopted in numerous areas such as laser imaging, image digitizing, projection displays [2] and medical applications, e.g. endoscopy and tomography. Features to be mostly considered for micromirrors include simple fabrication processes, low driving voltage, large tilt angle and linearized angular scan [3]. Actuation methods used for micromirrors include electrostatic [4–10], piezoelectric [11–17](PZT),electrothermal [18–20] and electromagnetic [21–24] actuators. Electrostatic actuation is the most popular actuation methods due to easy fabrication, low power consumption and high driving speed [25]. However, they require large operation voltages to have large tilting angles. Also for the MEMS devices that use parallel plate capacitors, pull in instability is a big concern [11, 26]. Electrothermal actuation mechanism provides large deflection angle for low voltage values, but their basic disadvantages are low driving speed and large energy consumption in addition to the change of optical behavior due to temperature [27,28]. Piezoelectric actuators have small device sizes, better response of driving speed compared to other actuators and low driving voltages [14–17]. However, they have the disadvantage of difficult fabrication. Electromagnetics actuators can achieve large mechanical tilting angle [23, 29] but at the price of larger size. Among these actuation types electrostatic actuator is preferred due to ease of fabrication in large volumes. Common electrostatic actuator types are comb-drive and parallel plate. Parallel plate actuators are preferred due to their smaller size compared to comb-drive actuators.

In this study an analytical model is investigated for a bi-axial micro-mirror. The model was introduced by Bai et al. [30], who developed an electrostatic micro-mirror with sidewall electrodes. They have presented simulations and experimental results. Contribution of this study is to simplify the analytical model presented [30] based on the independent excitation of the two rotation angles. we also changed the boundaries of the integral to account for the changes in the forces that become significant as the rotation angles increase.

The sidewall electrodes are used to decrease voltages and to increase rotation angles. The reason for adding sidewall electrodes is to increase the area of electrostatic force according to

*Address all correspondence to this author.

the electrostatic force equation $F = \frac{\varepsilon_0.A.V^2}{d^2}$ . Increasing forces on the mirror leads to larger torque around its axis of rotation and consequently larger rotation angle for the same amount of voltage. The micro-mirror structure consists of five main components; mirror plate, gimbal frame, sidewall electrode, bottom electrode and serpentine spring (torsion bar). The mirror is made of silicon and is connected to the ground and the voltage is applied to the sidewall and the bottom electrodes. Thus, the mirror is actuated by electrostatic forces generated from different potentials between the sidewall, the bottom electrodes and the mirror plate.

## 2 OPERATION PRINCIPLES

A schematic of the micro-mirror is shown in Figure 1. The micro-mirror is suspended by the double-gimbal structure, which has two pairs of serpentine springs (Figure 2) for 2 degree-of-freedom (DOF) scans: $\alpha$ and $\beta$ scan which are about x-axis and y-axis, respectively. The mirror actuators consist of four equivalent electrode quadrants (also sidewall electrodes) numbered as in Figure 1. The parameters of the micro-mirror are listed in Table 1. Different voltage potential between the mirror plate and the sidewall and bottom electrodes creates electrostatic torques that rotate the mirror. To operate the mirror, the two angles are excited independently. Voltages are applied to the sidewall and bottom electrodes of each quadrant according to the differential drive method suggested by Hao et al. [31] For the rotation about Y-axis ($\beta$)

$$\begin{aligned} V_1 = V_2 = V_{bias} + V_{dif} \\ V_3 = V_4 = V_{bias} - V_{dif} \end{aligned} \tag{1}$$

where $V_{bias}$ is the bias voltage and $V_{dif}$ is the differential voltage, and $V_{1...4}$ is the voltage on each quadrant. For the rotation about X-axis ($\alpha$)

$$\begin{aligned} V_1 = V_3 = V_{bias} - V_{dif} \\ V_2 = V_4 = V_{bias} + V_{dif} \end{aligned} \tag{2}$$

In other words, quadrants Q1 and Q2 will have equal and larger voltage compared to other quadrants to make the rotation angle $\beta$. Similarly, quadrants Q2 and Q4 will have equal and larger voltage compared to other quadrants to make the rotation angle $\alpha$.

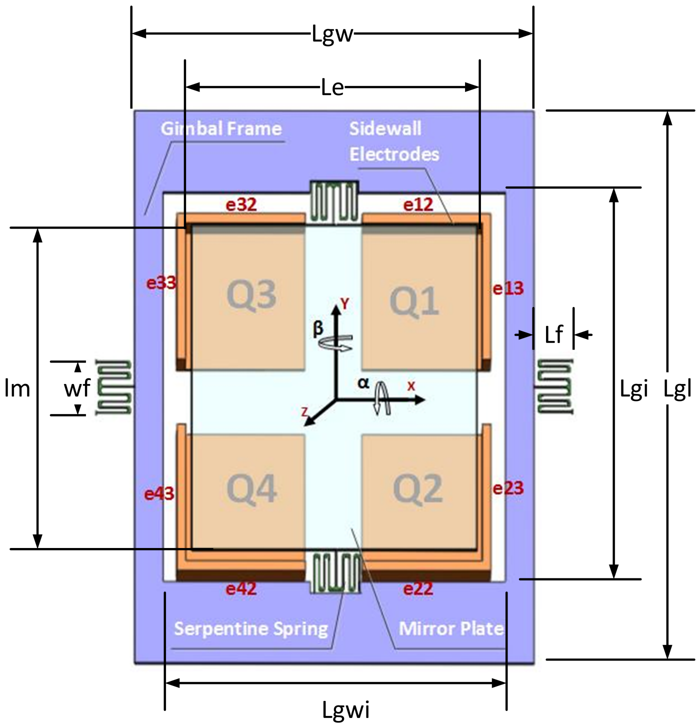


**FIGURE 1**: Mirror Elements and Quadrants

**FIGURE 2**: Serpentine Spring


## 3 SYSTEM MODEL

### 3.1 Electrostatic Forces and Torques

The global coordinate is XYZ and fixed at the center of the initial position of mirror center. The body fixed coordinate xyz is fixed at the center of the mirror plate and is rotating with the micro-mirror. Rotations about x and y axes are done independently. Using the defined coordinate systems, equations for forces and torques on the mirror from sidewall electrodes, gimbal frame and bottom electrodes are obtained, respectively in this section for angle $\alpha$. The derivation for angle $\beta$ is presented in the Appendix.

**3.1.1 Sidewall electrodes** Figure 3 shows the projection of the mirror plate on the YZ plane. The center of the mirror plate passes through the center of the global coordinate. The figure shows the mirror rotation about the X axis when quadrants 2 and 4 have equal and higher voltage than quadrants 1 and 3. In Figure 3, since the torques about the Y axis balance each other in this case, there will not be any rotation about the Y axis, so $\beta = 0$.

The model for electrostatic forces and torque here follow the procedure explained in Bai et. al [30], which consider the electrostatic forces from the sidewall 22 and 12 on the bottom surface of the mirror. However, we simplified the model based on the operation principle in the previous section (the two angles are operated independently). We also considered the electrostatic forces from the sidewall electrode on the top surface of the mirror as they become significant in large rotation angles. To incorporate this effect at large angles, the integral boundaries are defined that depend on the rotation angles obtained in the previous voltage step of the simulations.

For an element of dy on the top layer of the mirror plate, the electrostatic flux from sidewall 22 on the top surface of the mirror is written as;

$$E_{e22t} = \frac{V_2}{\overset{\frown}{AB}} \tag{3}$$

where $V_2$ is the voltage applied on quadrant 2 and

$$\begin{aligned} \overset{\frown}{AB} &= AC.(\pi/2-\alpha) = \frac{AD}{\sin(\pi/2-\alpha)}(\pi/2-\alpha) \\ &= (\frac{L_e}{2} - Y)\frac{\pi/2-\alpha}{\sin(\pi/2-\alpha)} \end{aligned} \tag{4}$$

Substituting $Y = y\cos\alpha$ for a body fixed point A, the flux equation 3 is written as;

$$E_{e22t} = \frac{V_2 \sin(\pi/2-\alpha)}{(\frac{L_e}{2} - y.\cos\alpha)(\pi/2-\alpha)} \tag{5}$$

The electrostatic pressure is

$$P = \frac{\varepsilon_0 E^2}{2} \tag{6}$$

Therefore the electrostatic force on on element with dimensions of dx and dy is

$$dF = \frac{\varepsilon_0 E^2 dxdy}{2} \tag{7}$$

**TABLE 1**: Parameters for micro-mirror structure [30] in Figures 1 and 2

| Parameter | Symbol | Value |
|---|---|---|
| Mirror Plate | | |
| Mirror width | lm | $1000\mu$ m |
| Mirror length | lm | $1000\mu$ m |
| Gimbal Frame | | |
| Outer width | Lgw | $1400\mu$ m |
| Inner width | Lgwi | $1200\mu$ m |
| Outer length | Lgl | $1700\mu$ m |
| Inner length | Lgi | $1200\mu$ m |
| Thickness | tg | 35 $\mu$ m |
| Width in Y direction | $g_{wy}$ | 250 $\mu$ m |
| Serpentine Spring | | |
| Width | w | 1.5-3 $\mu$ m |
| Thickness | $t_b$ | 12 $\mu$ m |
| $l_0$ | | 10 $\mu$ m |
| $l_p$ | | 110 $\mu$ m |
| $l_f$ | | 120 $\mu$ m |
| $l_i$ | | 120 $\mu$ m |
| $w_f$ | | 160 $\mu$ m |
| Electrode Dimensions | | |
| Bottom edge width | Le | 1060 $\mu$ m |
| Gap | g | 290 $\mu$ m |
| Sidewall thickness | $t_s$ | $40\mu$ m |
| Sidewall height | h | 250 $\mu$ m |
| Material Properties | | |
| Silicon density | $\rho$ | 2329 $kg/m^3$ |
| Young's Modulus | E | 79 Gpa |
| Shear Modulus | G | 73 Gpa |
| Air permittivity | $\varepsilon_0$ | $8.854e-12\frac{F}{m}$ |

The force in the Z direction from sidewall $e22$ is then found

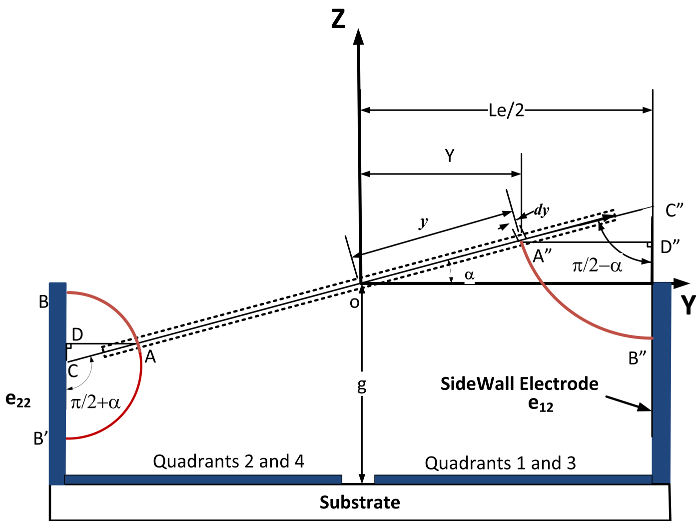


**FIGURE 3**: The mirror rotated about X axis by $\alpha$, and the sidewalls 12 and 22 projected on the YZ plane.

from integration

$$
\begin{aligned}
S_1 &= \frac{\varepsilon_0 . \sin^2(\pi/2-\alpha)}{2} \\
Fz_{e22t} &= \frac{S_1 V_2^2}{(\pi/2-\alpha)^2} . \int_{x_1}^{x_2} \int_{y_1}^{y_2} \left\{ \frac{1}{\frac{L_e}{2} - y.\cos\alpha} \right\}^2 .dxdy
\end{aligned} \tag{8}
$$

where $y_1 = \frac{Le}{2\cos(\alpha_0)} - \frac{Le}{2}\tan(\alpha_0)$, $y_2 = \frac{lm}{2}$, $x_1 = \frac{w_f}{2}$ and $x_2 = \frac{lm}{2}$, and $\alpha_0$ is the rotation angle in the previous voltage step. In other words, the boundaries of the integral changes as the rotation angle changes. At small angles, that does not make a difference in the results, but as the rotation angles grow, this effect becomes more significant.

From the force equation, one can find the torque about the x axis from sidewall $e22$ on top surface of the mirror plate.

$$
Tx_{e22t} = -\frac{S_1 V_2^2}{(\pi/2-\alpha)^2} . \int_{x_1}^{x_2} \int_{y_1}^{y_2} \left\{ \frac{1}{\frac{L_e}{2} - y.\cos\alpha} \right\}^2 .ydxdy \tag{9}
$$

For an element of dy at the bottom surface of the mirror plate (3), the electrostatic flux from sidewall $e22$ is written as;

$$
E_{e22b} = \frac{V_2}{\overset{\frown}{AB'}} \tag{10}
$$

where

$$
\begin{aligned}
\overset{\frown}{AB'} = AC.(\pi/2+\alpha) &= \frac{AD}{\sin(\pi/2-\alpha)}(\pi/2+\alpha) \\
&= \left(\frac{L_e}{2} - Y\right)\frac{\pi/2+\alpha}{\sin(\pi/2-\alpha)}
\end{aligned} \tag{11}
$$

Substituting $Y = y\cos\alpha$, the flux equation (10) is written as;

$$
E_{e22b} = \frac{V_2 \sin(\pi/2-\alpha)}{(\frac{L_e}{2} - y.\cos\alpha)(\pi/2+\alpha)} \tag{12}
$$

The force in the Z direction from sidewall $e22$ on the bottom part of the mirror is

$$
Fz_{e22b} = -\frac{S_1 V_2^2}{(\pi/2+\alpha)^2} . \int_{x_3}^{x_4} \int_{y_3}^{y_4} \left\{ \frac{1}{\frac{L_e}{2} - y.\cos\alpha} \right\}^2 .dxdy \tag{13}
$$

The boundaries of the integral can be found in Appendix B. The torque about the x axis from sidewall $e22$ at the bottom of the mirror plate is then

$$
Tx_{e22b} = \frac{S_1 V_2^2}{(\pi/2+\alpha)^2} . \int_{x_3}^{x_4} \int_{y_3}^{y_4} \left\{ \frac{1}{\frac{L_e}{2} - y.\cos\alpha} \right\}^2 .ydxdy \tag{14}
$$

Electrostatic forces from sidewall 12 also changes the rotation angle $\alpha$. As it can be seen from Figure 3, the electrostatic flux on the bottom surface of the mirror plate from side wall 12 is

$$
E_{e12} = \frac{V_1}{\overset{\frown}{A''B''}} = \frac{V_3}{A''C''.(\pi/2-\alpha)} \tag{15}
$$

where $V_1$ is the voltage of quadrant 1. The force and torque on the mirror plate from sidewall 12 can be derived similarly to equation (9) with different boundary for the integral.

$$
\begin{aligned}
Fz_{e12} &= -\frac{S_1 V_1^2}{(\pi/2-\alpha)^2} . \int_{x_5}^{x_6} \int_{y_5}^{y_6} \left\{ \frac{1}{\frac{L_e}{2} - y.\cos\alpha} \right\}^2 .dxdy \\
Tx_{e12} &= -\frac{S_1 V_1^2}{(\pi/2-\alpha)^2} . \int_{x_5}^{x_6} \int_{y_5}^{y_6} \left\{ \frac{1}{\frac{L_e}{2} - y.\cos\alpha} \right\}^2 .ydxdy
\end{aligned} \tag{16}
$$

Now we consider the effect of electrostatic forces from the sidewall electrodes on the gimbal frame which contributes to the rotation of the mirror. The gimbal frame does not rotate about Y axis based on Figure 4, and it can only rotate about X axis. That means the electrostatic forces generated between sidewalls and gimbal frame changes $\alpha$ angle only. Figure 4 shows the projection of the mirror plate and the gimbal frame on a plane parallel to YZ plane. Due to larger width of the gimbal frame in the y direction, only the electrostatic torques and forces caused by the sidewalls 12,22,32 and 42 are considered in the simulations.

The resulting electrostatic force in the Z direction and torque around the X axis caused by sidewall 12 forces on the top surface of the gimbal can be written:

$$\begin{aligned}
S_2 &= \frac{\varepsilon_0.\sin^2(\pi/2-\alpha)}{2} \\
Fz_{eg22t} &= \frac{S_2V_2^2}{(\pi/2+\alpha)^2}\int_{x_7}^{x_8}\int_{y_7}^{y_8}\left\{\frac{1}{y\cos\alpha-\frac{L_e}{2}-t_s}\right\}^2.dxdy \\
Tx_{eg22t} &= -\frac{S_2V_2^2}{(\pi/2+\alpha)^2}\int_{x_7}^{x_8}\int_{y_7}^{y_8}\left\{\frac{1}{y\cos\alpha-\frac{L_e}{2}-t_s}\right\}^2.ydxdy
\end{aligned} \tag{17}$$

It should be noted that the above equations are only valid when the angle of $\alpha$ is large enough so that integral boundaries $y_8 = Le/(2.\cos\alpha_0)+Le/2.\tan\alpha0 > y_7 = Lgl/2-g_{wy}$ and that happens when $\alpha_0 > 0.06$ radians. In other words, the forces on the top layer of gimbal frame only applies when the rotation angle $\alpha$ reaches certain value of 0.06 radians.

The sidewall 22 also exerts electrostatic forces on the bottom surface of the gimbal frame. The corresponding electrostatic force and torque are

$$\begin{aligned}
Fz_{eg22b} &= -\frac{S_2V_2^2}{(\pi/2-\alpha)^2}\int_{x_9}^{x_{10}}\int_{y_9}^{y_{10}}\left\{\frac{1}{y\cos\alpha-\frac{L_e}{2}-t_s}\right\}^2.dxdy \\
Tx_{eg22b} &= \frac{S_2V_2^2}{(\pi/2-\alpha)^2}\int_{x_9}^{x_{10}}\int_{y_9}^{y_{10}}\left\{\frac{1}{y\cos\alpha-\frac{L_e}{2}-t_s}\right\}^2.ydxdy
\end{aligned} \tag{18}$$

Similarly the electrostatic force and torque caused by sidewall 12 on the gimbal frame are

$$\begin{aligned}
Fz_{eg12} &= -\frac{S_2V_1^2}{(\pi/2+\alpha)^2}\int_{x_{11}}^{x_{12}}\int_{y_{11}}^{y_{12}}\left\{\frac{1}{y\cos\alpha-\frac{L_e}{2}-t_s}\right\}^2.dxdy \\
Tx_{eg12} &= -\frac{S_2V_1^2}{(\pi/2+\alpha)^2}\int_{x_{11}}^{x_{12}}\int_{y_{11}}^{y_{12}}\left\{\frac{1}{y\cos\alpha-\frac{L_e}{2}-t_s}\right\}^2.ydxdy
\end{aligned} \tag{19}$$

#### 3.1.2 Bottom Electrodes

The electrostatic forces and torques caused by bottom electrodes should also be added to the simulations. For the rotation angle $\alpha$, as it is shown in Figure 5, the flux can be obtained from

$$E_b = \frac{V}{\overset{\frown}{AB}} \tag{20}$$

where

$$\begin{aligned}
\overset{\frown}{AB} = AC.(\alpha) &= \frac{AD}{\sin(\alpha)}(\alpha) \\
&= (g+Y\tan\alpha)\frac{\alpha}{\sin(\alpha)}
\end{aligned} \tag{21}$$

Substituting $Y = y\cos\alpha$, and using the similar procedure as before, the electrostatic force and torque caused by voltages on quadrants 1 or 3 is derived

$$\begin{aligned}
S_3 &= \frac{\varepsilon_0.V_1^2}{2}\frac{\sin^2(\alpha)}{\alpha^2} \\
Fz_{eb1a} &= -S_3.\int_{x_{13}}^{x_{14}}\int_{y_{13}}^{y_{14}}\left(\frac{1}{g+y.\sin(\alpha)}\right)^2.dxdy \\
Tx_{eb1} &= -S_3.\int_{x_{13}}^{x_{14}}\int_{y_{13}}^{y_{14}}\left(\frac{1}{g+y.\sin(\alpha)}\right)^2.ydxdy
\end{aligned} \tag{22}$$

similarly, the electrostatic force and torque caused by bottom electrodes of quadrants 2 or 4 are

$$\begin{aligned}
S_4 &= \frac{\varepsilon_0.V_2^2}{2}\frac{\sin^2(\alpha)}{\alpha^2} \\
Fz_{eb2a} &= -S_3.\int_{x_{13}}^{x_{14}}\int_{y_{13}}^{y_{14}}\left(\frac{1}{g+y.\sin(\alpha)}\right)^2.dxdy \\
Tx_{eb2} &= S_3.\int_{x_{13}}^{x_{14}}\int_{y_{13}}^{y_{14}}\left(\frac{1}{g+y.\sin(\alpha)}\right)^2.ydxdy
\end{aligned} \tag{23}$$

For rotation angle $\beta$, the equations are derived in a similar fashion, except that the forces on the gimabl frame do not contribute to the rotation angle $\beta$, and therefore are not considered (Appendix A).

### 3.2 Mechanical Spring Force

When the micro-mirror is actuated by sidewall electrodes, the electrostatic forces and torques will be balanced by mechanical restoring forces and torques.

$$\begin{aligned}
&2.K_\alpha\alpha = 2(Tx_{e22t}+Tx_{e22b}+Tx_{e12}+(Tx_{eg22t}+Tx_{eg22b}) \\
&\quad +Tx_{eg12}+\textstyle\sum_{m=1}^{2}Tx_{ebm}) \\
&2.K_\beta\beta = 2(Ty_{e13t}+Tx_{e13b}+Ty_{e33}+Ty_{eb1}+Ty_{eb3}) \\
&K_zZ = 2(Fz_{e12}+Fz_{e22b}+Fz_{e22t}+Fz_{ge12}+Fz_{ge22b}+Fz_{ge22t} \\
&\quad +Fz_{eb1a}+Fz_{eb2a}+Fz_{e33}+Fz_{e13b}+Fz_{e13t}+Fz_{eb1b}+Fz_{eb3b})
\end{aligned} \tag{24}$$

In the above equations, the stiffness coefficients are doubled to account for the two springs resisting the motion about the two

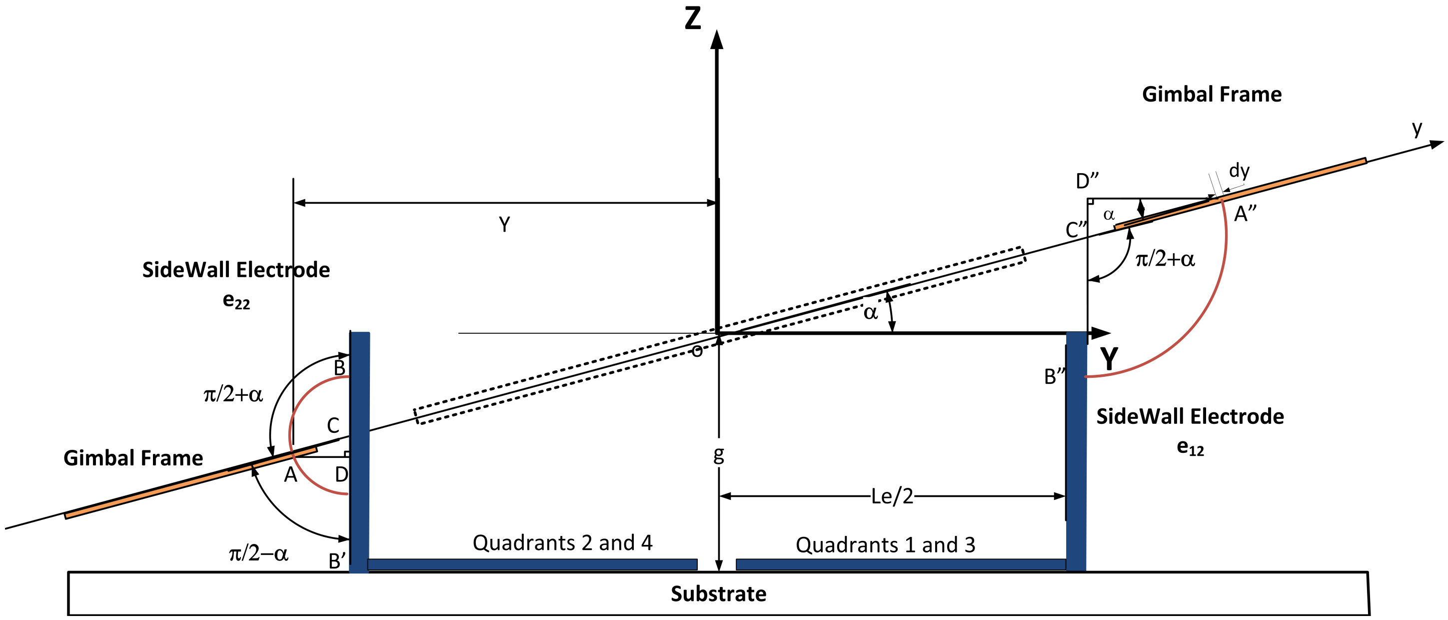


**FIGURE 4**: The Projection of the mirror plate, and gimbal and Sidewall electrodes on the YZ Plane

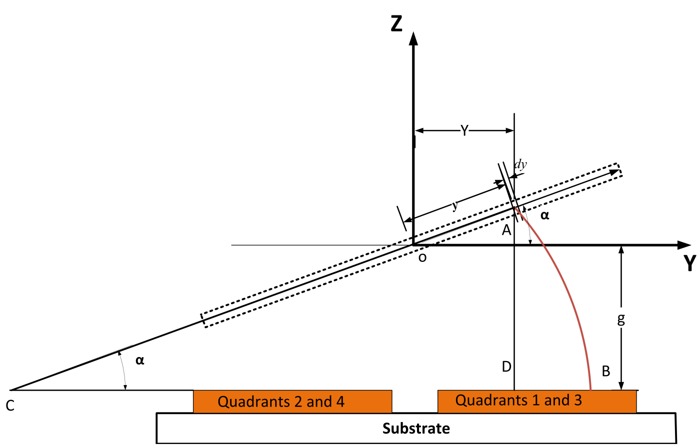


**FIGURE 5**: Bottom electrode effect for $\alpha$ scanning angle

axes. The serpentine spring has the stiffness [30] of

$$K_\alpha = K_\beta = \left( \frac{l_f + \frac{6}{4} l_p + \frac{2l_i}{4}}{G.J_r} + \frac{2l_0}{EI} \right)^{-1} \tag{25}$$

where for either of rotation angles, polar moment of inertia $J_r$, and moment of inertia of the spring rectangular cross section $I$ are

$$J_r = \frac{t_b^3.w}{3}.\left(1 - \frac{192 t_b}{w.\pi^5}.\tanh(\frac{\pi.w}{2t_b})\right)$$
$$I = \frac{w.t_b^3}{12} \tag{26}$$

For the simulations, displacement in the z directions are not illustrated and only the rotation angles are simulated using the equations 24 as described in the next section.

## 4 SIMULATION RESULTS

For obtaining the rotation angles, the summation of all the torques in corresponding directions of x and y are found considering the voltages of each quadrant. Equations 24 were solved at different differential voltages as indicated in equations 1 and 2. The displacement in the z direction has not been presented as the experimental data was not available for comparison. In the simulations, the fringe field effect is also considered negligible. Dimensions and material properties for the simulations, are listed in Table 1.

Figure 6 shows the comparison of the rotation angle $\alpha$ versus differential voltage based on the simplified analytical model and the experimental and simulation results [30]. $V_{bias}$ is applied as 55V and $V_{diff}$ ranges from 0-150V. It is noted the simplified model reveals close results for $\alpha$ scanning angle in Figure 6 compared with the reported results. However, unlike experiments, our model does not respond nonlinearly to the applied voltage at large angles. Nonlineartity in the response can be due to the gap decrease as the voltage increases. In our simulation, we assumed the gap is constant. More accurate model should account for changing of the gap as the voltage increases and using the calculated gap in the simulated rotation angles. This approach should make the curve nonlinear and similar to a regular pull-in curve.

Figure 7 shows the rotation angle $\beta$ versus differential voltage when bias voltage $v_{bia} = 55V$. It can be seen that the simplified model underestimate the scanning angles. For both rotation angles, we used the same mechanical stiffness for the springs and that can be the cause for deviation seen in the simulation of the rotation angle $\beta$. It is more likely that the mirror experiences more resistance in rotation about the X axis compared to the rotation about the Y axis. Overall, the model predicts the rotation angle $\alpha$ with more accuracy compared to the rotation angle $\beta$, which is underestimated.

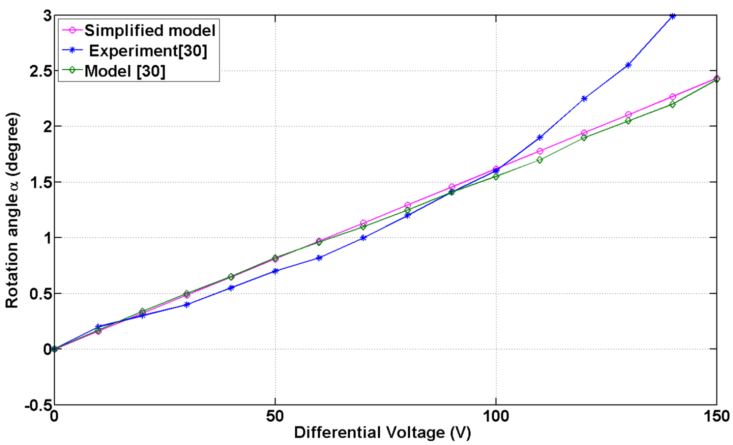


**FIGURE 6**: Alpha Scanning Angle when the $V_{bias} = 55V$

## 5 CONCLUSIONS

An analytical model for a bi-axial micro-mirror with side-wall electrodes is presented, which is a simplified model of a previous study [30] based on independent excitation of the two rotation angles. The mirror rotates about X and Y axes as a result electrostatic torques from different voltages on the mirror plate, side-wall electrodes, gimbal frame and the bottom electrodes. Actuation of the mirror is done using differential voltage excitation for the four quadrants and therefore, the rotations about axes are done independently which enabled simplifying the

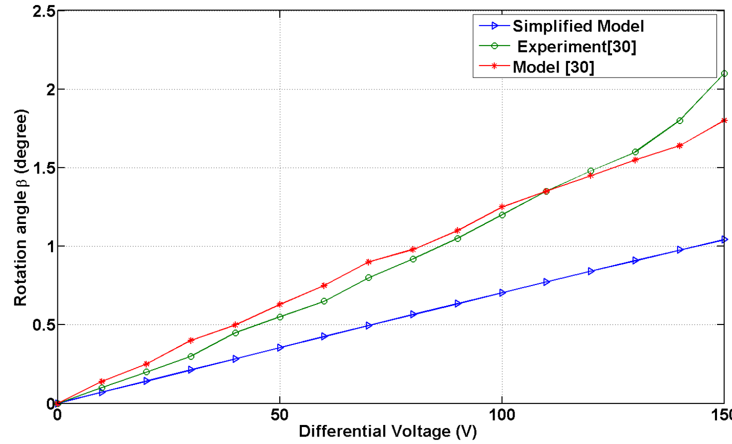


**FIGURE 7**: Beta Scanning Angle when the $V_{bias} = 55V$

equations. The integral boundaries are also chosen such that they account for forces applied on the mirror as the rotation angle increases. The simulation results of rotation angle about the X axis are in close proximity of the experiments, while simulation for rotation about Y axis underestimate the angles. Our future work accounts for the stiffness differences for rotations about the two axes. The simplified model with less computation time enables adding optimization algorithm, which was the motivation of this study to reduce the operating voltage and to increase the rotation angles.

## ACKNOWLEDGMENT

The authors would like to thank Turkish Military Academy (Ankara) for a PhD scholarship to support Mehmet Ozdogan for his research study.

## REFERENCES

[1] J. S. S. Rodgers, "Designing Microelectromechanical Systems-on-A Chip In a 5 Level Surface Technology," *Presented at the 2nd International Conference on Engineering Design and Automation*, 1998.
[2] M. Mignardi, "Digital micromirror array for projection TV," *Solid State Technology*, vol. 35, pp. 63–68, 1994.
[3] H. Toshiyoshi, W. Piyawattanametha, and M. Wu, "Linearization of electrostatically actuated surface micromachined 2-D optical scanner," *Journal of Microelectromechanical Systems*, vol. 10, pp. 205–214, June 2001.
[4] F. Hu, J. Yao, C. Qiu, and H. Ren, "A MEMS micromirror driven by electrostatic force," *Journal of Electrostatics*, vol. 68, pp. 237–242, June 2010.
[5] H. Moeenfard and M. T. Ahmadian, "Analytical modeling of bending effect on the torsional response of electrostat-

ically actuated micromirrors," *Optik - International Journal for Light and Electron Optics*, vol. 124, pp. 1278–1286, June 2013.

[6] F. Hu, Y. Tang, and Y. Qian, "Design of a MEMS micromirror actuated by electrostatic repulsive force," *Optik - International Journal for Light and Electron Optics*, vol. 123, pp. 387–390, Mar. 2012.

[7] W. Piyawattanametha, P. Patterson, D. Hah, H. Toshiyoshi, and M. Wu, "Surface- and bulk- micromachined two-dimensional scanner driven by angular vertical comb actuators," *Journal of Microelectromechanical Systems*, vol. 14, pp. 1329–1338, Dec. 2005.

[8] J. Singh, A. Agarwal, and M. Soundarapandian, "A novel electrostatic microactuator for large deflections in MEMS applications," *Thin Solid Films*, vol. 504, pp. 64–68, May 2006.

[9] S.-j. Chiou, T.-l. Hsieh, J.-c. Tsai, C.-W. Sun, D. Hah, and M. C. Wu, "A Two-Axis MEMS Scanner Driven by Radial Vertical Combdrive Actuators," *2007 IEEE/LEOS International Conference on Optical MEMS and Nanophotonics*, pp. 83–84, Aug. 2007.

[10] H. Xie, Y. Pan, and G. K. Fedder, "A CMOS-MEMS Mirror With Curled-Hinge Comb Drives," vol. 12, no. 4, pp. 450–457, 2003.

[11] K. H. Koh, T. Kobayashi, F.-L. Hsiao, and C. Lee, "Characterization of piezoelectric PZT beam actuators for driving 2D scanning micromirrors," *Sensors and Actuators A: Physical*, vol. 162, pp. 336–347, Aug. 2010.

[12] Y. Yee, H.-j. Nam, S.-h. Lee, J. U. Bu, and J.-w. Lee, "PZT actuated micromirror for ne-tracking mechanism of high-density optical data storage," vol. 89, pp. 166–173, 2001.

[13] A. Schroth, C. Lee, S. Matsumoto, and R. Maeda, "Application of solgel deposited thin PZT film for actuation of 1D and 2D scanners," no. April 1998, pp. 144–152, 1999.

[14] F. Filhol, E. Defaÿ, C. Divoux, C. Zinck, and M.-T. Delaye, "Resonant micro-mirror excited by a thin-film piezoelectric actuator for fast optical beam scanning," *Sensors and Actuators A: Physical*, vol. 123-124, pp. 483–489, Sept. 2005.

[15] J.-H. Park, J. Akedo, and H. Sato, "High-speed metal-based optical microscanners using stainless-steel substrate and piezoelectric thick films prepared by aerosol deposition method," *Sensors and Actuators A: Physical*, vol. 135, pp. 86–91, Mar. 2007.

[16] J. Janes, J. Quenzer, U. Hofmann, D. Kaden, and B. Wagne, " Design, Fabrication and Characterization of Low Voltage Piezoelectric Two Axis Gimbal-less Microscanners Fraunhofer Institu ute for Silicon Technology ISIT , Itzehoe , Ger rmany," no. June, pp. 2489–2492, 2013.

[17] W. Liao, W. Liu, J. E. Rogers, Y. Tang, B. P. Wang, and H. Xie, "A tip-tilt-piston piezoelectric scanning micromirror with folded PZT unimorph actuators," *2013 Transducers & Eurosensors XXVII: The 17th International Conference on Solid-State Sensors, Actuators and Microsystems (TRANSDUCERS & EUROSENSORS XXVII)*, vol. 1, pp. 526–529, June 2013.

[18] K. Ogando, N. La Forgia, J. Zárate, and H. Pastoriza, "Design and characterization of a fully compliant out-of-plane thermal actuator," *Sensors and Actuators A: Physical*, vol. 183, pp. 95–100, Aug. 2012.

[19] J. Singh, T. Gan, A. Agarwal, and S. Liw, "3D free space thermally actuated micromirror device," *Sensors and Actuators A: Physical*, vol. 123-124, pp. 468–475, Sept. 2005.

[20] L. Wu and H. Xie, "A scanning micromirror with stationary rotation axis and dual reflective surfaces for 360 forward-view endoscopic imaging," *TRANSDUCERS 2009 - 2009 International Solid-State Sensors, Actuators and Microsystems Conference*, pp. 2222–2225, June 2009.

[21] Z. Cui, X. Wang, Y. Li, and G. Y. Tian, "High sensitive magnetically actuated micromirrors for magnetic field measurement," *Sensors and Actuators A: Physical*, vol. 138, pp. 145–150, July 2007.

[22] C.-H. Ji, M. Choi, S.-C. Kim, K.-C. Song, J.-U. Bu, and H.-J. Nam, "Electromagnetic Two-Dimensional Scanner Using Radial Magnetic Field," *Journal of Microelectromechanical Systems*, vol. 16, pp. 989–996, Aug. 2007.

[23] Y. D. Gokdel, B. Sarioglu, S. Mutlu, and a. D. Yalcinkaya, "Design and fabrication of two-axis micromachined steel scanners," *Journal of Micromechanics and Microengineering*, vol. 19, p. 075001, July 2009.

[24] a.D. Yalcinkaya, H. Urey, D. Brown, T. Montague, and R. Sprague, "Two-Axis Electromagnetic Microscanner for High Resolution Displays," *Journal of Microelectromechanical Systems*, vol. 15, pp. 786–794, Aug. 2006.

[25] W. Jung, D. T. McCormick, J. Zhang, L. Wang, N. C. Tien, and Z. Chen, "Three-dimensional endoscopic optical coherence tomography by use of a two-axis microelectromechanical scanning mirror," *Applied Physics Letters*, vol. 88, no. 16, p. 163901, 2006.

[26] H. Moeenfard and M. T. Ahmadian, "A study of the static characteristics of a torsional micromirror," *Sensors and Actuators A: Physical*, vol. 90, pp. 73–81, May 2001.

[27] A. Jain, A. Kopa, Y. Pan, G. K. Fedder, and H. Xie, "A Two-Axis Electrothermal Micromirror for Endoscopic Optical Coherence Tomography," *IEEE Journal OF Selected Topics in Quantum Electronics*, vol. 10, no. 3, 2004.

[28] J. Singh, J. H. S. Teo, Y. Xu, C. S. Premachandran, N. Chen, R. Kotlanka, M. Olivo, and C. J. R. Sheppard, "A two axes scanning SOI MEMS micromirror for endoscopic bioimaging," *Journal of Micromechanics and Microengineering*, vol. 18, p. 025001, Feb. 2008.

[29] W. Makishi, Y. Kawai, and M. Esashi, "Magnetic torque driving 2D micro scanner with a non-resonant large scan angle," *Transducers*, June 2009.

[30] Y. Bai, J. T. W. Yeow, and B. C. Wilson, "Design , Fabri-

cation , and Characteristics of a MEMS Micromirror With Sidewall Electrodes," vol. 19, no. 3, pp. 619–631, 2010.
[31] Z. Hao, B. Wingfield, M. Whitley, J. Brooks, and J. Hammer, "A design methodology for a bulk-micromachined two-dimensional electrostatic torsion micromirror," *Journal of Microelectromechanical Systems*, vol. 12, pp. 692–701, Oct. 2003.

## Appendix A: Equations for rotation angle $\beta$

Sidewall 13 creates electrostatic forces on the top and bottom parts of the mirror plate. However, similar to rotation angle $\alpha$, the top forces only appear when the rotation angle $\beta$¿0.06 radians. For an element of dx on the top layer of the mirror plate (8), the electrostatic flux from sidewall 13 is written as;

$$E_{e13t} = \frac{V}{\overset{\frown}{AB}} \tag{27}$$

where

$$\begin{aligned} \overset{\frown}{AB} = AC.(\pi/2-\beta) &= \frac{AD}{\sin(\pi/2-\beta)}(\pi/2-\beta) \\ &= (\frac{L_e}{2}-X)\frac{\pi/2-\beta}{\sin(\pi/2-\beta)} \end{aligned} \tag{28}$$

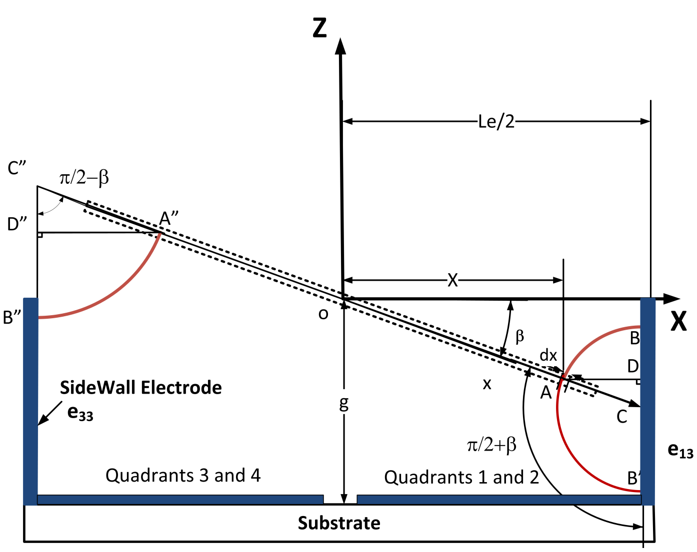


**FIGURE 8**: The mirror rotated about Y axis by $\beta$, and the sidewalls 13 and 33 projected on the XZ plane.

Substituting $X = x\cos\beta$ for a body fixed point A, the flux equation 27 is written as;

$$E_{e13t} = \frac{V.\sin(\pi/2-\beta)}{(\frac{L_e}{2}-x.\cos\beta)(\pi/2-\beta)} \tag{29}$$

The electrostatic pressure is

$$P = \frac{\varepsilon_0 E^2}{2} \tag{30}$$

Therefore the electrostatic force on on element with dimensions dx and dy is

$$dF = \frac{\varepsilon_0 E^2 dxdy}{2} \tag{31}$$

The electrostatic force in the Z direction and the torque about the Y axis from sidewall $e13$ on top surface of the mirror plate are then obtained.

$$\begin{aligned} S_5 &= \frac{\varepsilon_0.\sin^2(\pi/2-\beta)}{2} \\ Fz_{e13t} &= \frac{S_5 V_1^2}{(\pi/2-\beta)^2}.\int_{y15}^{y16}\int_{x15}^{x16}\left\{\frac{1}{\frac{L_e}{2}-x.\cos\beta}\right\}^2.dxdy \\ Ty_{e13t} &= -\frac{S_5 V_1^2}{(\pi/2-\beta)^2}.\int_{y15}^{y16}\int_{x15}^{x16}\left\{\frac{1}{\frac{L_e}{2}-x.\cos\beta}\right\}^2.xdxdy \end{aligned} \tag{32}$$

For an element of dx at the bottom surface of the mirror plate (8), the electrostatic flux from sidewall 13 is written as;

$$E_{e13b} = \frac{V_1}{\overset{\frown}{AB'}} \tag{33}$$

where

$$\begin{aligned} \overset{\frown}{AB'} = AC.(\pi/2+\beta) &= \frac{AD}{\sin(\pi/2-\beta)}(\pi/2+\beta) \\ &= (\frac{L_e}{2}-X)\frac{\pi/2+\beta}{\sin(\pi/2-\beta)} \end{aligned} \tag{34}$$

Substituting $X = x\cos\beta$ for a body fixed point, the flux equation (33) is written as;

$$E_{e13b} = \frac{V_1\sin(\pi/2-\beta)}{(\frac{L_e}{2}-x.\cos\beta)(\pi/2+\beta)} \tag{35}$$

The force and torque equations are then derived

$$
\begin{aligned}
Fz_{e13b} &= -\frac{S_5 V_1^2}{(\pi/2+\beta)^2}.\int_{y17}^{y18}\int_{x17}^{x18}\left\{\frac{1}{\frac{L_e}{2}-x.\cos\beta}\right\}^2.dxdy \\
Ty_{e13b} &= \frac{S_5 V_1^2}{(\pi/2+\beta)^2}.\int_{y17}^{y18}\int_{x17}^{x18}\left\{\frac{1}{\frac{L_e}{2}-x.\cos\beta}\right\}^2.xdxdy
\end{aligned} \tag{36}
$$

Electrostatic forces from sidewall 33 also changes the rotation angle $\beta$. The force and torque on the mirror plate from sidewall 33 can be derived similarly to equation (32) with different boundary for the integral.

$$
\begin{aligned}
Fz_{e33} &= -\frac{S_5 V_3^2}{(\pi/2-\beta)^2}.\int_{y19}^{y20}\int_{x19}^{x20}\left\{\frac{1}{\frac{L_e}{2}-x.\cos\beta}\right\}^2.dxdy \\
Ty_{e33} &= -\frac{S_5 V_3^2}{(\pi/2-\beta)^2}.\int_{y19}^{y20}\int_{x19}^{x20}\left\{\frac{1}{\frac{L_e}{2}-x.\cos\beta}\right\}^2.xdxdy
\end{aligned} \tag{37}
$$

The forces and torques generated by bottom electrode of quadrants 1 or 2 to change $\beta$ angle (9) are

$$
\begin{aligned}
S_6 &= \frac{\varepsilon_0.V_1^2}{2}\frac{\sin^2(\beta)}{\beta^2} \\
Ty_{eb1} &= S_6.\int_{y21}^{y22}\int_{x21}^{x22}\left(\frac{1}{g-x.\sin(\beta)}\right)^2.xdxdy \\
Fz_{eb1b} &= -S_6.\int_{y21}^{y22}\int_{x21}^{x22}\left(\frac{1}{g-x\sin(\beta)}\right)^2.dxdy
\end{aligned} \tag{38}
$$

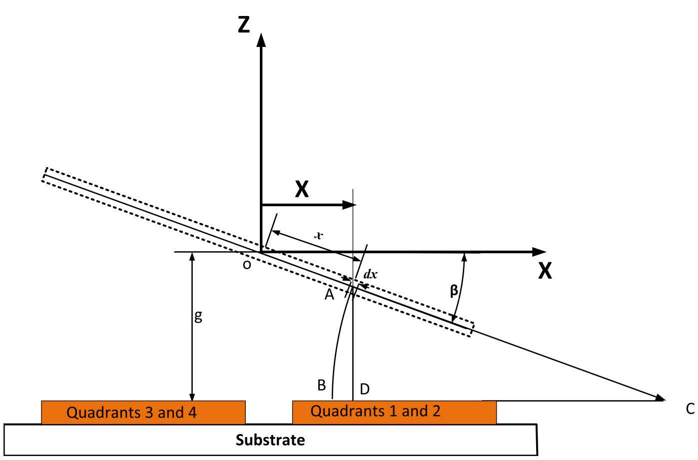


**FIGURE 9**: Bottom electrode effect for $\beta$ scanning angle

## Appendix B: Integral Boundaries

$$y_1 = \frac{Le}{2\cos(\alpha_0)} - \frac{Le}{2}\tan(\alpha_0) \qquad y_2 = \frac{lm}{2}$$

$$x_1 = \frac{w_f}{2} \qquad x_2 = \frac{lm}{2}$$

$$y_3 = \frac{Le}{2\cos(\alpha_0)} - g + \frac{Le}{2}\tan(\alpha_0) \qquad y_4 = \frac{lm}{2}$$

$$x_3 = \frac{w_f}{2} \qquad x_4 = \frac{lm}{2}$$

$$y_5 = \frac{w_f}{2} \qquad y_6 = \frac{lm}{2}$$

$$x_5 = \frac{w_f}{2} \qquad x_6 = \frac{lm}{2}$$

$$y_7 = \frac{Lgl}{2} - g_{wy} \qquad y_8 = \frac{Le}{2\cos(\alpha_0)} + \frac{Le}{2}\tan(\alpha_0)$$

$$x_7 = \frac{w_f}{2} \qquad x_8 = \frac{Le}{2} + t_s$$

$$y_9 = \frac{Lgl}{2} - g_{wy} \qquad y_{10} = \frac{Le}{2\cos(\alpha_0)} + g - \frac{Le}{2}\tan(\alpha_0)$$

$$x_9 = \frac{w_f}{2} \qquad x_{10} = \frac{Le}{2} + t_s$$

$$y_{11} = \frac{Lgl}{2} - g_{wy} \qquad y_{12} = \frac{Le}{2\cos(\alpha_0)} + \frac{Le}{2}\tan(\alpha_0) + g$$

$$x_{11} = \frac{w_f}{2} \qquad x_{12} = \frac{Le}{2} + t_s$$

$$y_{13} = \frac{w_f}{2} \qquad y_{14} = \frac{lm}{2}$$

$$x_{13} = \frac{w_f}{2} \qquad x_{14} = \frac{lm}{2}$$

$$x_{15} = \frac{Le}{2\cos(\alpha_0)} - \frac{Le}{2}\tan(\alpha_0) \qquad x_{16} = \frac{lm}{2}$$

$$y_{15} = \frac{w_f}{2} \qquad y_{16} = \frac{lm}{2}$$

$$x_{17} = \frac{-Le}{2} + g \qquad x_{18} = \frac{lm}{2}$$

$$y_{17} = \frac{w_f}{2} \qquad y_{18} = \frac{lm}{2}$$

$$x_{19} = \frac{Le}{2} - g \qquad x_{20} = \frac{lm}{2}$$

$$y_{19} = \frac{w_f}{2} \qquad y_{20} = \frac{lm}{2}$$

$$x_{21} = \frac{w_f}{2} \qquad x_{22} = \frac{lm}{2}$$

$$y_{21} = \frac{w_f}{2} \qquad y_{22} = \frac{lm}{2}$$